

Montclair State University
Montclair State University Digital Commons

Department of Earth and Environmental Studies
Faculty Scholarship and Creative Works

Department of Earth and Environmental Studies

9-2019

A geomorphic enthalpy method: Description and application to the evolution of fluvial-deltas under sea-level cycles

William Anderson
Montclair State University

Jorge Lorenzo Trueba
Montclair State University, lorenzotruej@mail.montclair.edu

Vaughan Voller
University of Minnesota

Follow this and additional works at: <https://digitalcommons.montclair.edu/earth-environ-studies-facpubs>



Part of the [Applied Mathematics Commons](#), and the [Earth Sciences Commons](#)

MSU Digital Commons Citation

Anderson, William; Lorenzo Trueba, Jorge; and Voller, Vaughan, "A geomorphic enthalpy method: Description and application to the evolution of fluvial-deltas under sea-level cycles" (2019). *Department of Earth and Environmental Studies Faculty Scholarship and Creative Works*. 56.

<https://digitalcommons.montclair.edu/earth-environ-studies-facpubs/56>

Published Citation

Anderson, W., Lorenzo-Trueba, J., & Voller, V. (2019). A geomorphic enthalpy method: Description and application to the evolution of fluvial-deltas under sea-level cycles. *Computers & Geosciences*, 130, 1–10. <https://doi.org/10.1016/j.cageo.2019.05.006>

This Postprint is brought to you for free and open access by the Department of Earth and Environmental Studies at Montclair State University Digital Commons. It has been accepted for inclusion in Department of Earth and Environmental Studies Faculty Scholarship and Creative Works by an authorized administrator of Montclair State University Digital Commons. For more information, please contact digitalcommons@montclair.edu.

1 **A geomorphic enthalpy method: Description and application to the evolution**
2 **of fluvial-deltas under sea-level cycles**

3
4 William Anderson¹, Jorge Lorenzo-Trueba^{2*}, Vaughan Voller³

5
6 ¹ Department of Mathematical Sciences, Montclair State University, Montclair, USA

7 ² Department of Earth and Environmental Studies, Montclair State University, Montclair, USA

8 ³ Department of Civil Engineering, University of Minnesota, Minneapolis, USA

9
10 * Corresponding author: Jorge Lorenzo-Trueba. Email address: lorenzotruej@montclair.edu

11 * Corresponding author address: CELS 302, 1 Normal Ave, Montclair State University,
12 Montclair, NJ 07043.

13 Link to the code: <https://github.com/JorgeMSU/1D-enthalpy-method>

14 Highlights:

- 15 • Enthalpy-like solution to study fluvio-deltaic dynamics under sea-level variations.
16 • Model produces stratigraphic profiles under a wide range of sea-level curves.
17 • Time lags in system response can lead to river incision during the sea-level rise.

18
19
20
21
Authorship statement: WA and JLT developed the theory and performed the computations with input from VV. JLT and WA wrote the manuscript with input from VV. JLT designed and directed the project.

22 **Abstract**

23 Fluvial deltas are composites of two primary sedimentary environments: a depositional fluvial
24 region and an offshore region. The fluvial region is defined by two geomorphic moving
25 boundaries: an alluvial-bedrock transition (ABT), which separates the sediment prism from the
26 non-erodible bedrock basement, and the shoreline (SH), where the delta meets the ocean. The
27 trajectories of these boundaries in time and space define the evolution of the shape of the
28 sedimentary prism, and are often used as stratigraphic indicators, particularly in seismic studies,
29 of changes in relative sea level and the identification of stratigraphic sequences. In order to better
30 understand the relative role of sea-level variations, sediment supply, and basin geometry on the
31 evolution of the ABT and SH, we develop a forward stratigraphic model that accounts for
32 curvature changes of the fluvial surface and treats the SH and ABT as moving boundaries (i.e.,
33 internal boundaries that are not known a priori and their location must be calculated as part of the
34 solution to the overall problem). This forward model extends a numerical technique from heat
35 transfer (i.e., enthalpy method), previously applied to the evolution of sedimentary basins, to
36 account for sea-level variations, including eustatic sea-level cycles. In general, model results
37 demonstrate the importance of the dynamics of the fluvial surface on the system response under
38 a large range of input parameter values. Specifically, model results suggest that time lags in the
39 ABT response during sea-level cycles can result in geologically long-lived river incision in the
40 upper and mid portions of the fluvial surface during sea-level rise. These results suggest that the
41 relationship between the coastal onlap configuration of strata and relative changes in sea level is
42 complex, and therefore not necessarily a good indicator of contemporaneous sea-level changes.

43

44 Keywords: Enthalpy method, Fluvial deltas, sea-level cycles, Alluvial-basement transition,
45 Shoreline, river incision

46 **1. Introduction**

47 Fluvial deltas are composites of several basic environments, including a depositional fluvial
48 region and a subaqueous offshore region, that generally resemble a triangular prism
49 superimposed upon a relatively planar basement profile (Figure 1a; Chavarrías et al., 2018;
50 Lorenzo-Trueba et al., 2009; Paola, 2000; Posamentier et al., 1992; Swenson et al., 2005). This
51 triangular sedimentary prism presents three geomorphic boundaries or vertices: the alluvial-
52 bedrock transition (ABT), which separates the bedrock (or basement) from the depositional
53 fluvial region, the shoreline (SH), which separates the fluvial region from the subaqueous
54 depositional region, and the delta toe where the subaqueous sediment wedge intersects with the
55 basement. Changes in the length of the depositional fluvial domain occur via transgression (i.e.,
56 SH landwards migration), regression (i.e., SH seawards migration), coastal onlap (i.e., ABT
57 landwards migration), and coastal offlap (i.e., ABT seawards migration) (see Figure 1). These
58 changes are in general a function of the sediment supply to the sedimentary prism, the efficacy of
59 the sediment transport and deposition along the fluvial surface, and relative sea-level variations
60 (i.e., the combination of eustatic sea level changes and subsidence). For instance, if sediment
61 supply is high relative to both the length of the fluvial surface and the accommodation created by
62 sea-level rise, the results is SH regression and coastal onlap, which causes an overall lengthening
63 of the sedimentary prism, as well as an increase in elevation (i.e., river aggradation) of the fluvial
64 surface (Figure 1b). A combination of relative sea-level fall with low sediment supply, however,
65 typically results in regression, coastal offlap, and a decrease in elevation (i.e., river degradation)
66 of the fluvial surface (Figure 1c). Additionally, Muto and Steel (2002) found that a low sediment

67 supply relative to the length of the fluvial surface and the rate of relative sea-level rise can lead
68 to a break in the triangular geometry of the sedimentary prism as the system transgresses (Figure
69 1d).

70

71 Cycles of SH transgression/regression and coastal onlap/offlap in the sedimentary record (Figure
72 1) can potentially allow for reconstruction of a basin's history of sediment supply and paleo-sea
73 level (Henriksen et al., 2009; Törnqvist et al., 2006). To tackle this inverse problem, the
74 migration of the internal boundaries that describe the evolution of the system (e.g., ABT, SH)
75 have to be computed as a part of the solution to the overall geological problem (Lorenzo-Trueba
76 et al., 2013, 2009; Lorenzo-Trueba and Voller, 2010; Marr et al., 2000; Swenson et al., 2000).

77 Analogous to the migration of the ice/water front in a one phase Stefan melting problem (Crank,
78 1984), Swenson et al. (2000) applied this framework to the migration of the SH in sedimentary
79 basins. In particular, these authors used an analogy between heat and sediment diffusive
80 transport to describe the movement of the SH under varying conditions of sediment supply and
81 relative sea level. Follow-up work by Voller et al. (2004) found that in the particular case of
82 constant sediment supply and a fixed sea level, the problem presented by Swenson et al. (2000)
83 allows for a closed-form analytical solution. Based on Voller et al. (2004), Capart et al. (2007),
84 and Lai and Capart (2007) developed analytical solutions in which the ABT and the SH were
85 treated as independent moving boundaries. Lorenzo-Trueba et al. (2009) expanded on this work
86 by developing an analytical solution able to track both the ABT and the SH under conditions of
87 constant sediment supply and fixed sea-level. Lorenzo-Trueba et al. (2009) also validated this
88 solution against flume experiments under a range of system parameters. In addition to studying
89 the kinematics of ocean shoreline deltas, similar models and solution methodologies along the

90 lines of those noted above, have also been applied in studies of lake deltas and morphology, e.g.,
91 (Capart et al., 2010).

92

93 Although simplified solutions can increase the clarity and insights the model facilitates, moving
94 boundary problems only have analytical solutions in a limited range of scenarios. In order to
95 study more general cases, different numerical methods have been developed for the dual ABT
96 and SH moving boundary problem (Lorenzo-Trueba and Voller, 2010; Parker et al., 2008; Voller
97 et al., 2006). Parker et al. (2008) developed a deforming grid method, based on a Landau front-
98 fixing approach, able to track both the ABT and the SH under constant sea-level rise in a one-
99 dimensional setting. A drawback of the deforming grid method, however, is that the extension to
100 two-dimensions is far from straightforward. Voller et al. (2006) developed a solution based on
101 the enthalpy method, able to operate on a fixed grid under constant sea level, and focused on the
102 dynamics of the SH. Lorenzo-Trueba and Voller (2010) extended this numerical solution to
103 account for the migration of both the ABT and SH. Despite these recent developments, however,
104 to date all numerical solutions had been restricted to either a fixed sea level or constant sea-level
105 rise scenarios. The only attempt to solve the problem under sea-level cycles was by Lorenzo-
106 Trueba et al. (2013), who developed an integral approximation of the Exner equation assuming a
107 quadratic fluvial surface profile. This solution, however, is not able to account for full cycles of
108 transgression and regression (only cases where transgression follows regression). Thus, our first
109 goal is to extend the enthalpy-like numerical solution from Lorenzo-Trueba and Voller (2010) to
110 account for sea-level cycles, as well as cycles of SH transgression/regression. Second, we
111 investigate potential modes of coastal behavior under sea-level cycles and a wide range of
112 system parameters.

113

114 **2. The Dual Moving Boundary Problem**

115 **2.1 Equations**

116

117 We model fluvio-deltaic evolution in cross-section as described in Figure 2a. As opposed to
118 previous modeling efforts that account for different shoreface morphologies (Lai and Capart,
119 2007; Swenson et al., 2005), temporal changes in sediment supply (An et al., 2017), or breaks in
120 the basement slope (Lai et al., 2017), we assume a linear basement slope β , a linear foreset slope
121 ψ , and a steady sediment supply q_0 . We adopt this idealized cross-shore geometry to simplify the
122 calculations and focus on the role of the fluvial surface dynamics on the response of the system.
123 Given such cross-shore geometry (Figure 2), the evolution of the fluvio-deltaic system can be
124 described in terms of the locations of the ABT ($x = r(t)$), the SH ($x = s(t)$), and the delta toe
125 ($x = w(t)$). In the absence of differential subsidence, we can describe changes in the elevation h
126 at any location of the fluvial surface with respect to current sea level (Figure 2a) as the
127 divergence of the sediment flux q (Paola and Voller, 2005),

$$128 \quad \frac{\partial h}{\partial t} = -\frac{\partial q}{\partial x}, \quad r(t) \leq x \leq s(t) \quad (1)$$

129 where x is positive in the seaward direction, and $x=0$ is located at the intersection between the
130 initial sea level and the basement.

131 Following numerous efforts, which include both numerical modeling and laboratory experiments
132 (Paola et al., 1992; Ribberink and van der Sande, 1985; Fagherazzi and Overeem, 2007; Parker
133 and Muto, 2003; Postma et al., 2008; Swenson et al., 2000; Swenson and Muto, 2007), we
134 assume that q is primarily controlled by the fluvial slope. In particular, for simplicity we assume

135 that q is linearly related to the fluvial slope as follows (Paola et al., 1992; Lorenzo-Trueba et al.,
136 2013; Lorenzo-Trueba and Voller, 2010; Marr et al., 2000; Swenson et al., 2000; Swenson and
137 Muto, 2007)

$$138 \quad q(x) = -v \frac{\partial h}{\partial x} \quad (2)$$

139 where v is the ‘fluvial diffusivity’, which can be calculated as a function of water discharge and
140 grain size characteristics (Paola, 2000).

141

142 The combination of equations (1) and (2) leads to the so-called linear diffusion equation, which
143 generally requires two boundary conditions and an initial condition to be solved. In this case,
144 however, the locations of the ABT and the SH (i.e., r and s) are unknown a priori and need to be
145 solved as part of the solution. Consequently, the problem requires four boundary conditions
146 instead of just two. The first condition matches the fluvial surface elevation at the ABT to the
147 basement elevation:

$$148 \quad h|_{x=r} = -\beta r \quad (3a)$$

149 The second condition implies that the elevation of the fluvial surface at the SH is equal to sea
150 level:

$$151 \quad h|_{x=s} = Z \quad (3b)$$

152 where Z is the sea level. The third condition imposes a given sediment input q_0 at the ABT:

$$153 \quad -v \frac{\partial h}{\partial x} \Big|_{x=r} = q_0 \quad (3c)$$

154 The fourth condition in general relates the sediment flux that reaches the SH with the rate of
 155 migration of the foreset toe, which is defined as $dw/dt = ds/dt + 1/\psi \cdot dZ/dt$ (Swenson et
 156 al., 2000). In the particular case in which the shoreface toe only migrates seawards (i.e.,
 157 $dw/dt > 0$), the system maintains the wedge geometry depicted in Figure 1, and we can define
 158 the basin depth as $D(x, t) = \psi/(\psi - \beta) \cdot (s\beta + Z)$ (Lorenzo-Trueba et al., 2013). For
 159 simplicity, however, given that the foreset slope ψ is generally orders of magnitude larger than
 160 any other slope in the system, including the basement slope β , we assume $\psi/(\psi - \beta) \sim 1$
 161 (Edmonds et al., 2011; Lorenzo-Trueba et al., 2013, 2009; Lorenzo-Trueba and Voller, 2010;
 162 Swenson and Muto, 2007). This assumption implies that a shift from regression to transgression
 163 coincides with the abandonment of the subaqueous foreset, which means that the SH and the
 164 delta toe always migrate in the same direction (i.e., $dw/dt = ds/dt$). In this scenario, the fourth
 165 boundary relates the sediment flux that reaches the SH with the rate of migration of the SH and
 166 the ocean depth as follows:

$$167 \quad -v \left. \frac{\partial h}{\partial x} \right|_{x=s} = \begin{cases} D(x, t) \frac{ds}{dt}, & \frac{ds}{dt} > 0 \\ 0, & \frac{ds}{dt} \leq 0 \end{cases} \quad (3d)$$

168 When the SH migrates seawards (i.e., $ds/dt > 0$) beyond past SH locations, the system
 169 maintains the wedge geometry and the basin depth reduces to $D(x, t) = s\beta + Z$. In contrast,
 170 when all sediments deposit on the fluvial surface before reaching the SH, the SH sediment flux is
 171 equal to zero and the SH migrates landwards (i.e., $ds/dt \leq 0$). Under this condition, the SH
 172 detaches from the subaqueous foreset (Figure 2b), a condition previously defined as ‘autobreak’
 173 (Muto and Steel, 2002). Additionally, in some instances the SH migrates seaward (i.e., $ds/dt >$

174 0) over subaqueous deposits left during autobreak, in which case $D(x, t)$ corresponds to the
175 ocean depth of these offshore deposits (Figure 2c).

176 Under these conditions, with equations (1-3) and a given initial geometry: $s(0) = r(0) = 0$, we
177 can fully describe the dynamics of the fluvial surface under sea-level changes, including cycles
178 of regression and transgression (Figure 2).

179

180 **2.2 A dimensionless form**

181 In this section, we reduce the number of controlling parameters to a minimum by rewriting the
182 governing equations (1-3) in dimensionless form. The scaling used towards this end is as follows

$$183 \quad x^d = \frac{x}{l}, \quad t^d = \frac{t}{\tau}, \quad s^d = \frac{s}{l}, \quad r^d = \frac{r}{l}, \quad Z^d = \frac{Z}{l\beta}, \quad h^d = \frac{h}{l\beta}, \quad D^d = \frac{D}{l\beta}, \quad q^d = \frac{q\tau}{l^2\beta} \quad (4)$$

184 where l is the horizontal scale (e.g., a characteristic delta length), $l\beta$ is the vertical scale, and $\tau =$
185 l^2/v is an ‘equilibrium timescale’ defined by Paola et al. (1992). From the scaling in (4), we
186 obtain one dimensionless group: the ratio of the fluvial to the bedrock slope at the ABT

$$187 \quad R_{ab} = -\frac{1}{\beta} \frac{\partial h}{\partial x} \Big|_{x=r} = \frac{q_0}{\beta v} \quad (5)$$

188 which is physically constrained within the range $0 < R_{ab} < 1$.

189 Dropping the d superscript for convenience of notation, the
190 dimensionless versions of equations (1) to (3) become:

$$191 \quad \frac{\partial h}{\partial t} = \frac{\partial^2 h}{\partial x^2}, \quad r(t) \leq x \leq s(t) \quad (6)$$

192 with conditions

193 $h|_{x=r} = -r$ (7a)

194 $h|_{x=s} = Z$ (7b)

195 $-\frac{\partial h}{\partial x}\Big|_{x=r} = R_{ab}$ (7c)

196 $-\frac{\partial h}{\partial x}\Big|_{x=s} = \begin{cases} D(x, t) \frac{ds}{dt}, & \frac{ds}{dt} > 0 \\ 0, & \frac{ds}{dt} \leq 0 \end{cases}$ (7d)

197 The initial conditions are:

198 $s(t = 0) = r(t = 0) = 0$. (8)

199 In the particular case in which the SH only migrates seawards (i.e., $ds/dt > 0$), the system
 200 maintains the wedge geometry depicted in Figures 1a and 2a, and we can define the basin depth
 201 as $D(x, t) = s + Z$ (Lorenzo-Trueba et al., 2013). Under this special case, equations (6) – (8)
 202 admit close form analytical solutions, which are described in section 4. In general, however,
 203 these equations require a numerical solution.

204

205 **3. The Geomorphic Enthalpy Method**

206 In this section, we develop a numerical solution able to operate in cases where the closed form
 207 solutions do not hold. Moreover, the objective of this section is to present a fixed grid enthalpy-
 208 like method that solves the problem numerically without the need of tracking the ABT and the
 209 SH as part of the solution (Voller et al. 2006; Lorenzo-Trueba and Voller 2010). With this
 210 objective in mind, we define the enthalpy function $H(x, t)$, which in our case represents the
 211 sediment prism thickness (Figure 3), as follows:

212 $H(x, t) = h(x, t) + Z(t) - E(x)$ (9)

213 where $E(x)$ denotes the basement elevation, i.e., $E(x) = -x$. Inverting (9), we can describe the
 214 elevation respect to current sea level (Figure 2a) anywhere in the domain as follows

215 $h = \max(H + E - Z, 0)$. (10)

216 As defined by equation (10), h is always greater than zero landward of the SH, and zero
 217 seawards of the SH (Figure 3). Consequently, sediment fluxes as described in equation (2) are
 218 zero beyond the SH, which implies that the subaqueous portion of the fluvial-delta maintains its
 219 sediment thickness and hence its shape. Although we believe this is a reasonable assumption to
 220 first order, future versions of the model will investigate the effect of waves and tides on the
 221 transport of sediments in the subaqueous portion.

222 Equations (9) and (10) are fully consistent with the original enthalpy formulation introduced by
 223 Crank (1984). However, as previously noted by Voller et al. (2006) and Lorenzo-Trueba and
 224 Voller (2010), in this case the term representing the latent heat $L(x, t) = Z(t) - E(x)$ can be a
 225 function of space and time. Using equations (9) and (10), we can then describe the problem using
 226 the same sediment balance equation for the full solution space, i.e.,

227 $\frac{\partial H}{\partial t} = -\frac{\partial q}{\partial x}, \quad -\infty \leq x \leq \infty$ (11)

228 where q is the sediment flux described in equation (2). At the upstream limit of the domain, the
 229 sediment flux is always equal to the sediment input, which in dimensionless numbers is equal to
 230 R_{ab} , i.e., $\lim_{x \rightarrow -\infty} q = R_{ab}$. At the downstream limit of the domain, the elevation above sea level is
 231 always equal to zero, i.e., $\lim_{x \rightarrow \infty} h = 0$. Equation (11) also requires initial conditions to be solved,
 232 which we define as follows

233 $H(x, 0) = 0$ (12a)

234 $h(x, 0) = \begin{cases} -x, & x < 0 \\ 0, & x \geq 0 \end{cases}$ (12b)

235 We develop a numerical solution for equations (9) to (12) based on a uniform grid size Δx and
 236 time step size Δt . We set the origin point $x = 0$, where the ABT and SH are located initially, at
 237 the interface between two nodes in the center of the domain (Figure 4). We set the index i for the
 238 first node landward of the origin to be equal to zero. The value of i increases as we move
 239 seaward, and decreases and becomes negative as we move landwards. In general, we can express
 240 the location of node i as $x_i = (i - 0.5) \cdot \Delta x$.

241 We discretize equation (11) at node i using the following finite differences form

242 $H_{i,j+1} = H_{i,j} + \frac{\Delta t}{\Delta x} \cdot \left(q_{i+\frac{1}{2},j} - q_{i-\frac{1}{2},j} \right)$ (13)

243 where the superscript j refers to the time step, and the subscript $i+1/2$ refers to the interface
 244 between nodes i and $i+1$. This equation guarantees that sediment is conserved in every node of
 245 the entire domain. Additionally, we compute the flux from node i to node $i+1$ at time step j as

246 $q_{i+\frac{1}{2},j} = \min \left(H_{i,j} \frac{\Delta x}{\Delta t} + q_{i-\frac{1}{2},j}, \frac{h_{i,j} - h_{i+1,j}}{\Delta x} \right)$ (14)

247 We note that the formulation introduced by equation (14) departs from the formulation
 248 introduced by Lorenzo-Trueba and Voller (2010) (i.e., $q_{i+\frac{1}{2},j} = \min(R_{ab}, (h_{i,j} - h_{i+1,j})/\Delta x)$).
 249 Lorenzo-Trueba and Voller's formulation only works when the ABT solely migrates landwards
 250 and sediment deposition takes place along the fluvial surface on every cell and time step.
 251 Consequently, in this particular scenario sediment flux q is bounded above by the upstream

252 sediment supply in dimensionless form (i.e., $q \leq R_{ab}$). In the more general case presented here,
 253 however, we can simulate sediment erosion on the fluvial surface, as well as seaward migration
 254 of the ABT. In this case, under the assumption of a non-erodible basement, sediment flux
 255 $q_{i+\frac{1}{2},j}$ is bounded above by the sum of the sediment input to the upstream cell $q_{i-\frac{1}{2},j}$ and the total
 256 sediment volume in the upstream cell $H_{i,j}\Delta x/\Delta t$.

257 In order to guarantee stability, the time and space steps need to satisfy $\Delta t/\Delta x^2 < 0.5$. To meet
 258 this stability criterion, we generally use a space step $\Delta x = 0.01$ and a time step in the
 259 range $10^{-5} \leq \Delta t \leq 5 \cdot 10^{-5}$. Higher resolution may be needed to ensure accuracy for high
 260 values of R_{ab} .

261 At each time step, the solution of (13) explicitly provides new values for the sediment
 262 thickness $H_{i,j+1}$ at each node. We then calculate the values at the new time step for the sediment
 263 heights $h_{i,j+1}$ from the discrete form of equation (12). With this information, we can calculate
 264 the sediment fluxes using equation (14), and move to the next time step to solve again equation
 265 (13).

266 Additionally, although not required, we can determine the position of the ABT at each time step
 267 by searching left to right through the domain and finding the first cell i where $q_{i-\frac{1}{2},j} \neq q_{i+\frac{1}{2},j}$.
 268 This cell represents the most landward location where sediment deposition occurs, i.e., the cell
 269 immediately seaward of the ABT. We then estimate the ABT position by interpolating between
 270 nodes i and $i - 1$ as follows:

$$271 \quad r_j = \frac{h_{i,j} + Z_j + R_{ab}x_i}{1 - R_{ab}}. \quad (15)$$

272 We can also estimate the location of the SH at each time step. Under SH progradation, the
273 current total sediment field $H_{i,j}$ is searched, and the first node i where $0 < H_{i,j} + E_i < Z_j$ is
274 located. The SH position is then determined by interpolation through the control volume around
275 node i , i.e.

$$276 \quad s_j = (i - 1)\Delta x - \frac{H_{i,j}}{E_i - Z_j} \Delta x . \quad (16)$$

277

278 **4. Verification of the enthalpy method**

279 We verify the proposed model under two sea-level change scenarios that admit closed form
280 analytical solutions: square-root sea-level rise and fall, and constant sea-level rise. Under the
281 condition of sea-level change proportional to the square root of time i.e., $Z = 2\lambda_z\sqrt{t}$, Lorenzo-
282 Trueba et al. (2013) developed an analytical similarity solution in which the movements of the
283 ABT and SH are given by equations of the form: $r = -2\lambda_{ab}\sqrt{t}$ and $s = 2\lambda_{sh}\sqrt{t}$, where λ_{ab} and
284 λ_{sh} are constants determined through the solution of two algebraic equations (Lorenzo-Trueba et
285 al., 2013). We use this analytical solution to assess accuracy of the enthalpy method under a
286 wide range of λ_z and R_{ab} scenarios (see Appendix). In this section, we present two examples that
287 demonstrate model performance under both ABT seaward and landward migration, including
288 their profile evolution (Figure 5).

289

290 Under a constant sea-level rise rate \dot{z} (i.e., sea level is described as $Z = \dot{z} \cdot t$), the system
291 eventually reaches a point at which all incoming sediment deposit on the fluvial surface in order
292 to keep pace with sea-level rise (Muto, 2001; Parker and Muto, 2003) , which results in the
293 fluvial plain abandoning the foreset or submarine portion (Figure 2b). When this happens, the

294 system first enters a transition period in which the length of the fluvial plain increases and both
295 the ABT and the SH migrate landwards. This transition period ends when the fluvial surface
296 attains a fixed geometry, and both the ABT and the SH attain a constant landward migration rate.
297 At this point, the geometry of the fluvial surface, as well as the ABT and SH trajectories, can be
298 described analytically (a full derivation of this solution is included in the Appendix). We use this
299 analytical solution to test the fixed grid numerical scheme for a wide range of R_{ab} and \dot{z} values.
300 In all scenarios, there is agreement between the analytical and numerical solutions (see
301 Appendix).

302

303 **5. System response to sea-level cycles: The importance of fluvial surface dynamics**

304 Numerous studies over the past few decades present sea-level change as the most important
305 allogenic (i.e., external) forcing affecting coastal areas such as fluvial deltas and coastal margins
306 (Blum et al., 2013; Catuneanu et al., 2009; Van Wagoner et al., 1990; Van Wagoner and
307 Bertram, 1995), and consequently as the primary control on stratigraphic architecture. While
308 evidence for incised (paleo) valley systems formed during oscillations in sea level during the
309 Quaternary is extensive (Blum et al., 2013; Blum and Törnqvist, 2000), the range of sea-level
310 cycle amplitudes and frequencies stored in the stratigraphic record remains unclear (Li et al.,
311 2016). In this section, we demonstrate how the proposed enthalpy method can be used to bring
312 some light to this question by exploring the dynamics and stratigraphy of the system under sea-
313 level variations. In particular, we go beyond the scenarios investigated in the model verification
314 and explore the system response under sinusoidal sea-level cycles, i.e.,

$$315 \quad Z = A \sin(B \cdot t) \quad (17)$$

316 where A and B are the dimensionless amplitude and frequency (i.e., 1/period) of the sea-level
317 cycles. We select a representative length scale $l = 100\text{km}$, a basement slope $\beta = 10^{-3}$, and a
318 diffusivity $\nu = 10^5\text{m}^2\text{y}^{-1}$ associated with a catchment length of $\sim 100\text{ km}$ (Swenson et al., 2000).
319 In this way, we can use the dimensional scaling described in equation (4) to calculate the
320 amplitude and period of sea-level cycles using the A and B values. For instance, $A=1$ and $B=1$
321 correspond to sea-level cycles of 100m in amplitude and a period of 100,000 years, which are
322 comparable to quaternary-scale eccentricity-driven eustatic sea level cycles (Hajek and Straub,
323 2017). Lower A and B values (e.g., $A=0.3$ and $B=0.4$) better match with late Miocene conditions,
324 when obliquity cycles ($\sim 40\text{ ky}$) resulted in sea changes with ranges of 10–35 m.

325

326 An interesting feature under sea-level cycles is that the SH can reverse its direction of migration.
327 During these reversals, the geometric configuration of the system shifts between the one shown
328 in Figure 2a, in which wedge geometry is maintained, and Figure 2b, in which the foreset and the
329 fluvial plain abandons the submarine portion (i.e., autobreak). This is well illustrated in Figures 6
330 and 7, which demonstrate that the geomorphic enthalpy method introduced here can account for
331 transgression followed by regression and vice versa. Figure 6 includes three stratigraphic profiles
332 produced by the model that demonstrate the effect of R_{ab} on the system response. As we
333 increase R_{ab} , which is proportional to the sediment supply (see equation (5)), the magnitude and
334 occurrence of river incision (i.e., ABT seaward migration) and SH transgression are reduced, and
335 there is larger preservation of sedimentary deposits. The formation and evolution of each of these
336 stratigraphic profiles is included in the supplementary material, and Figure 7a includes the ABT
337 and SH trajectories for the scenario depicted in Figure 6c (medium R_{ab} value).

338

339 Figures 6 and 7 (and videos in the supplementary material) also illustrate the importance of the
340 dynamics of the fluvial surface on the ABT and SH responses. During the sea-level rise phase,
341 the relief of the fluvial surface decreases and its convexity increases as a large fraction of the
342 sediment input deposits on the subaerial portion of the sedimentary prism. In contrast, under sea-
343 level fall the relief and concavity of the fluvial surface increase as a larger fraction of sediments
344 bypass the subaerial portion of the delta to build the foreset. These shifts in the curvature and
345 relief of the fluvial surface can delay the response of the system to sea-level variations. In
346 particular, the transition from a concave and seaward migrating fluvial surface profile during sea-
347 level fall to a convex and lower relief fluvial surface during the sea-level rise can result in river
348 incision during the sea-level rise (Figures 6-7a); Lorenzo-Trueba et al. (2013) first reported this
349 interesting phenomenon. Additionally, the transition from a convex fluvial surface profile during
350 the sea-level rise stage to a concave profile during the sea-level fall stage can result in the
351 truncation of sediment layers in the nearshore region, leaving ‘lenses’ of older sediment
352 surrounded by newer sediments (Figure 6). It is important to note that neither of these two
353 behaviors can be captured by models that impose a linear fluvial slope (Kim and Muto, 2007;
354 Lorenzo-Trueba et al., 2012), or the general sequence stratigraphic model, which assumes a fixed
355 fluvial surface profile that translates seaward and landward, tracking the regressing and
356 transgressing SH (Posamentier and Vail, 1988).

357

358 To further explore the time lags in system response, we define the ABT and SH residuals (i.e.,
359 s_{res} and r_{res}) as the difference between the ABT and SH trajectories under sea-level cycles and
360 the corresponding trajectories under constant sea level (Figure 7a). By plotting the residual
361 trajectories with the sea-level curve (Figure 7b and 7c), we find that SH response is typically in

362 phase with sea level such that maxima and minima in the SH trajectory correspond
363 approximately to minima and maxima in sea level, respectively. In contrast, delays in the ABT
364 response to sea-level variations can be geologically long-lived, and can result in river incision
365 that prolongs into the sea-level rise stage (Figure 8 and 9). Such time delays increase as R_{ab}
366 increases, and can reach values of hundreds of thousands of years, but barely change as a
367 function of the amplitude of the sea-level oscillations A (Figure 8a). River incision during sea-
368 level rise, however, can only occur when A is at least large enough to cause river incision during
369 the fall stage, which can then extend into the sea-level rise stage. Thus, the total sediment
370 volume eroded (i.e., river incision) under sea-level rise increases as A increases (Figure 8b), and
371 represents a significant fraction of the total sedimentary wedge volume under high amplitude
372 sea-level oscillations (Figure 9).

373
374 The relationship between the sediment volume eroded during sea-level rise and R_{ab} is more
375 complex (Figure 8b). Under low to medium values of R_{ab} , the seaward migration of the ABT
376 drives river incision (Figure 9b and 9c). In this case, as R_{ab} increases, the longer the seaward
377 migration of the ABT prolongs beyond the sea-level fall stage into the sea-level rise stage, which
378 in turn results in a higher sediment volume eroded. Under medium to high values of R_{ab} ,
379 however, the ABT can maintain its landward migration even under extended periods of sea-level
380 fall, and river incision occurs instead due to curvature changes of the fluvial surface (Figure 9d).
381 In this scenario, an increase in R_{ab} , which is proportional to the sediment supply (see equation
382 (5)), tends to reduce the sediment volume eroded under sea-level cycles.

383

384 **6. Discussion and future work**

385 Numerous field, experimental, and theoretical studies have been conducted to date to understand
386 how allogenic controls such as sea-level change influence stratigraphy (Allen, 1978; Armitage et
387 al., 2011; Heller et al., 2001; Heller and Paola, 1996; Hickson et al., 2005; Martin et al., 2011,
388 2009; van Heijst and Postmal, 2001; Van Wagoner et al., 1990). Despite all these efforts, which
389 provide a sound conceptual framework for interpreting ancient deposits, there exist fundamental
390 gaps regarding the relationship between processes, stratigraphy, and fluvial-deltaic evolution. In
391 this manuscript, we address this knowledge gap by developing and verifying a fixed grid
392 enthalpy-like numerical solution aimed to explore the evolution of fluvial deltas under a wide
393 range of scenarios. The novelty of this modeling framework, which can be viewed as a
394 generalized one-dimensional Stefan problem with two geomorphic moving boundaries (i.e., the
395 ABT and the SH), is that the “latent heat” (which resembles ocean depth in our case) can change
396 both in time and space. As a result, this model can for the first time incorporate sea-level cycles,
397 as well as cycles of SH transgression/regression.

398

399 Model results in this manuscript do not aim at specifically reproducing the evolution of any
400 particular fluvial delta, and therefore do not capture the complexities associated with multiple
401 grain sizes, sediment compaction, or deep crustal processes. The model also assumes that the
402 evolution of the system can be described in a one-dimensional longitudinal section, leaving out
403 processes such as river avulsions, which can play a role on the large-scale evolution of the
404 system. These model simplifications, however, allow us to focus our analysis on the interplay
405 between sediment supply, sea-level changes, and the dynamics of the fluvial surface.
406 Additionally, given the simplicity of the model we can explore the effect of this interplay under a
407 wide range of system parameters.

408

409 Overall, model results demonstrate the potential of numerical heat transfer methods, specifically
410 those developed to solve moving boundary problems, to advance our understanding of the
411 formation and evolution of sedimentary basins. Model results also demonstrate that the dynamics
412 of the fluvial surface can play an essential role on the system response to sea-level variations.
413 Previous studies have highlighted the importance of autogenic storage and release processes
414 during a full sea-level cycle, such that periods of sea-level rise are not purely depositional while
415 periods of sea-level fall are also not purely erosional (Blum and Price, 1998; Holbrook, 2001;
416 Strong and Paola, 2008). To the best of our knowledge, however, this is the first study that
417 relates changes in the relief and concavity of the fluvial surface profile during sea-level cycles
418 with the occurrence of geologically long-lived (i.e., thousands of years) river incision during sea-
419 level rise. Moreover, the model predicts that the volume of sediment eroded during river incision
420 under sea-level rise significantly increases as the amplitude of the sea-level oscillations increase.
421 Future work will aim at narrowing down the conditions and past sea-level changes that could
422 make such behavior likely. Additionally, we are planning to carry out laboratory-scale flume
423 experiments to validate the model results. The next step in terms of numerical modeling will be
424 to extend the geomorphic enthalpy model into two dimensions.

425

426 **Acknowledgments**

427 We thank the donors of the American Chemical Society Petroleum Research Fund for support of
428 this research (PRF #58817-DNI8). We also thank two anonymous reviewers for their valuable
429 comments.

430

431

432 **Computer Code Availability**

433 The code “1D enthalpy method”, developed by William Anderson and Jorge Lorenzo-Trueba
434 can be accessed since October 2018 at <https://github.com/JorgeMSU/1D-enthalpy-method>. For
435 details about this code, contact Jorge Lorenzo-Trueba via email (lorenzotruej@montclair.edu) or
436 by phone (973-655-5320). Jorge Lorenzo-Trueba’s office is at 1 Normal ave., Montclair State
437 University, NJ 07043. The code is less than 200 lines, it can run in a standard laptop, and is
438 written in matlab.

439

440

441 **Appendix A: Additional verification of the enthalpy method.**

442 In this section, we include further testing of the fixed grid numerical scheme under two sea-level
443 change scenarios that admit closed form analytical solutions: square-root sea-level rise and fall,
444 and constant sea-level rise.

445

446 *A.1 Square-root sea-level rise and fall*

447

448 Under the condition of sea-level change proportional to the square root of time i.e., $Z = 2\lambda_z\sqrt{t}$,
449 Lorenzo-Trueba et al. (2013) developed an analytical similarity solution in which the movements
450 of the ABT and SH are given by equations of the form:

$$451 \quad r = -2\lambda_{ab}\sqrt{t} \tag{A1a}$$

$$452 \quad s = 2\lambda_{sh}\sqrt{t} \tag{A1b}$$

453 where λ_{ab} and λ_{sh} are constants determined through the solution of two algebraic equations
454 (Lorenzo-Trueba et al., 2013). We use this analytical solution to assess accuracy of the enthalpy
455 method under a wide range of R_{ab} and λ_Z values. Figure 5 shows plots of the SH and ABT
456 trajectories over time for two values of R_{ab} during sea-level fall. In both scenarios, there is
457 agreement between the analytical and numerical solutions. Depending on both R_{ab} and the value
458 of λ_Z the delta can undergo coastal offlap or coastal onlap during sea-level fall. The profile
459 evolutions in figure 5 illustrate differences in concavity of the fluvial surface that are a result of
460 the direction of ABT migration. In scenarios of sea-level fall proportional to the square root of
461 time larger values of R_{ab} or smaller values of λ_Z result in coastal onlap and a concave up fluvial
462 surface. However, significantly decreasing R_{ab} or increasing the magnitude of λ_Z causes the
463 delta to undergo coastal offlap and produces a concave down fluvial surface. During costal offlap
464 sediments are reworked in the upstream portion of the delta and provided to the rest of the
465 system causing sediment flux values in the fluvial surface to exceed R_{ab} and resulting in the
466 concave downward profile. Model runs for several values of R_{ab} and λ_Z are included in figures
467 A1 and A2.

468 A further test of the robustness of the enthalpy solution is revealed by investigating its
469 performance across the entire feasible range of the ABT slope ratio $0 < R_{ab} < 1$; in each case
470 the value of λ_Z is set proportional to λ_{sh} . First, the analytical solution in Lorenzo-Trueba et al.
471 2012 is used to predict values of λ_{ab} and λ_{sh} . Then, we extract the values of λ_{ab} and λ_{sh} at
472 specific values of R_{ab} [0.05: 0.05: 0.95] through fitting the forms in (9) to the predicted
473 trajectories r and s given by the enthalpy solution. Benchmarks are made for both a sea-level
474 rise (e.g., $\lambda_Z = 0.5\lambda_{sh}$) and a sea-level fall (e.g., $\lambda_Z = -0.5\lambda_{sh}$). In Figure A3 we present a
475 comparison of the analytical values of the moving boundary parameters (solid-line) with those

476 predicted by the enthalpy method (shapes). We find that across a wide range of conditions the
477 time stepping solution matches the analytical solution.

478

479 *A.2 Constant sea-level rise*

480

481 Under a constant sea-level rise rate \dot{z} (i.e., sea level is described as $Z = \dot{z} \cdot t$), the system can
482 reach a point in which the incoming sediment flux is insufficient to supply the foreset (Muto,
483 2001; Parker and Muto, 2003), which results in the fluvial plain abandoning the submarine
484 portion (Figure 2b). When this happens, the system first enters a transition period in which the
485 length of the fluvial plain increases and both the ABT and the SH migrate landwards. This
486 transition period ends when the fluvial surface attains a fixed geometry, and both the ABT and
487 the SH attain a constant landward migration rate. At this point, the problem admits an analytical
488 solution as the fluvial-surface attains a fixed geometry that migrates landwards at a given speed.
489 We can then describe such analytical solution by setting the following similarity variable:

$$490 \quad \xi = x + \dot{z}t, \quad (A2a)$$

491 scale the sediment height by

$$492 \quad \eta = h - \dot{z}t, \quad (A2b)$$

493 and define the following location for the boundaries of the fluvial surface

$$494 \quad s^* = s_i - \dot{z}t \quad (A3a)$$

$$495 \quad r^* = r_i - \dot{z}t. \quad (A3b)$$

496 In this way, the similarity solution becomes

497 $\frac{d^2\eta}{d\xi^2} - \dot{z} \frac{d\eta}{d\xi} - \dot{z} = 0, \quad r^* \leq \xi \leq s^*$ (A4)

498 with boundary conditions

499 $\eta|_{\xi=s^*} = 0$ (A5a)

500 $\eta|_{\xi=r^*} = -r^*$ (A5b)

501 $\frac{\partial\eta}{\partial\xi}\Big|_{\xi=r^*} = -R_{ab}$ (A5c)

502 $\frac{\partial\eta}{\partial\xi}\Big|_{\xi=s^*} = 0.$ (A5d)

503 On satisfying (A3), (A4a), and (A4d) we obtain the following solution

504 $\eta = \frac{1}{\dot{z}} \exp(\dot{z}\xi - \dot{z}s^*) - \xi + \frac{R_{ab}-1}{\dot{z}}$ (A6a)

505 $h = \frac{1}{\dot{z}} \exp(\dot{z}x - \dot{z}s) - x + \frac{R_{ab}-1}{\dot{z}}.$ (A6b)

506 From (2) and (3) we obtain the values of s^* , and r^*

507 $s^* = \frac{R_{ab}}{\dot{z}}$ (A7a)

508 $r^* = \frac{1}{\dot{z}} [R_{ab} + \ln(1 - R_{ab})].$ (A7b)

509 Thus, the length of the fluvial surface can be calculated as

510 $s^* - r^* = s_i - r_i = \frac{\ln(1-R_{ab})}{\dot{z}}.$ (A8)

511 We use this analytical solution to test the fixed grid numerical scheme for a wide range of

512 R_{ab} and \dot{Z} values. Figure A4 shows plots of the movement of the SH and ABT over time. We

513 find that the trajectories predicted by the enthalpy solution (solid-lines) eventually match the
514 analytical solution (dashed-line).

515 Additionally, further test of the robustness of the enthalpy solution is revealed by investigating
516 its performance across the entire feasible range of the ABT slope ratio $0 < R_{ab} < 1$. In
517 particular, we calculate the length of the fluvial surface at steady state (i.e., $s-r$) for specific
518 values of R_{ab} [0.05: 0.05: 0.95], using the enthalpy solution and the analytical solution (equation
519 (A7)). In Figure A5 we present a comparison of the analytical values of the moving boundary
520 parameters (solid-line) with those predicted by the enthalpy method (shapes). We find that across
521 a wide range of conditions the time stepping solution matches the analytical solution.

522

523

524

525

526

527

528

529 **References**

530 Allen, J.R.L., 1978. Studies in fluvial sedimentation: an exploratory quantitative model for the
531 architecture of avulsion-controlled alluvial suites. *Sediment. Geol.* 21, 129–147.

532 [https://doi.org/10.1016/0037-0738\(78\)90002-7](https://doi.org/10.1016/0037-0738(78)90002-7)

533 An, C., Cui, Y., Fu, X., Parker, G., 2017. Gravel-bed river evolution in earthquake-prone regions
534 subject to cycled hydrographs and repeated sediment pulses. *Earth Surf. Process. Landforms*
535 42, 2426–2438. <https://doi.org/10.1002/esp.4195>

536 Armitage, J.J., Duller, R.A., Whittaker, A.C., Allen, P.A., 2011. Transformation of tectonic and
537 climatic signals from source to sedimentary archive. *Nat. Geosci.* 4, 231–235.
538 <https://doi.org/10.1038/ngeo1087>

539 Blum, M., Martin, J., Milliken, K., Garvin, M., 2013. Paleovalley systems: Insights from
540 Quaternary analogs and experiments. *Earth-Science Rev.* 116, 128–169.
541 <https://doi.org/10.1016/j.earscirev.2012.09.003>

542 Blum, M.D., Price, D.M., 1998. Relative Role of Eustasy, Climate, and Tectonism in Continental
543 Rocks. *Quat. Alluv. Plain Constr. Response to Glacio-eustatic Clim. Control. Texas Gulf*
544 *Coast. Plain* 59, 31–48.

545 Blum, M.D., Törnqvist, T.E., 2000. Fluvial responses to climate and sea-level change: A review
546 and look forward. *Sedimentology* 47, 2–48. [https://doi.org/10.1046/j.1365-](https://doi.org/10.1046/j.1365-3091.2000.00008.x)
547 [3091.2000.00008.x](https://doi.org/10.1046/j.1365-3091.2000.00008.x)

548 Capart, H., Bellal, M., Young, D.-L., 2007. Self-Similar Evolution of Semi-Infinite Alluvial
549 Channels with Moving Boundaries. *J. Sediment. Res.* 77, 13–22.
550 <https://doi.org/10.2110/jsr.2007.009>

551 Capart, H., Hsu, J., Lai, S., Hsieh, M., 2010. Formation and decay of a tributary-dammed lake,
552 Laonong River, Taiwan. *Water Resour. Res.* 46.

553 Catuneanu, O., Abreu, V., Bhattacharya, J.P., Blum, M.D., Dalrymple, R.W., Eriksson, P.G.,

554 Fielding, C.R., Fisher, W.L., Galloway, W.E., Gibling, M.R., Giles, K.A., Holbrook, J.M.,
555 Jordan, R., Kendall, C.G.S.C., Macurda, B., Martinsen, O.J., Miall, A.D., Neal, J.E.,
556 Nummedal, D., Pomar, L., Posamentier, H.W., Pratt, B.R., Sarg, J.F., Shanley, K.W., Steel,
557 R.J., Strasser, A., Tucker, M.E., Winker, C., 2009. Towards the standardization of sequence
558 stratigraphy. *Earth-Science Rev.* 92, 1–33. <https://doi.org/10.1016/j.earscirev.2008.10.003>

559 Chavarrías, V., Blom, A., Orrú, C., Martín-Vide, J.P., Viparelli, E., 2018. A Sand-Gravel Gilbert
560 Delta Subject to Base Level Change. *J. Geophys. Res. Earth Surf.* 123, 1160–1179.
561 <https://doi.org/10.1029/2017JF004428>

562 Crank, J., 1984. *Free and Moving Boundary Problems*. Oxford Press.

563 Edmonds, D.A., Paola, C., Hoyal, D.C.J.D., Sheets, B.A., 2011. Quantitative metrics that
564 describe river deltas and their channel networks. *J. Geophys. Res. Earth Surf.* 116, 1–15.
565 <https://doi.org/10.1029/2010JF001955>

566 Fagherazzi, S., Overeem, I., 2007. Models of Deltaic and Inner Continental Shelf Landform
567 Evolution. *Annu. Rev. Earth Planet. Sci.* 35, 685–715.
568 <https://doi.org/10.1146/annurev.earth.35.031306.140128>

569 Hajek, E.A., Straub, K.M., 2017. Autogenic Sedimentation in Clastic Stratigraphy. *Annu. Rev.*
570 *Earth Planet. Sci.* 45, 681–709. <https://doi.org/10.1146/annurev-earth-063016-015935>

571 Heller, P.L., Paola, C., 1996. Downstream Changes in Alluvial Architecture: An Exploration of
572 Controls on Channel-Stacking Patterns. *J. Sediment. Res.* 66, 297–306.
573 <https://doi.org/10.1306/D4268333-2B26-11D7-8648000102C1865D>

574 Heller, P.L., Paola, C., Hwang, I.G., John, B., Steel, R., 2001. Geomorphology and sequence

575 stratigraphy due to slow and rapid base-level changes in an experimental subsiding basin
576 (XES96-1). *Am. Assoc. Pet. Geol. Bull.* 85, 817–838. [https://doi.org/10.1306/8626CA0F-](https://doi.org/10.1306/8626CA0F-173B-11D7-8645000102C1865D)
577 [173B-11D7-8645000102C1865D](https://doi.org/10.1306/8626CA0F-173B-11D7-8645000102C1865D)

578 Henriksen, S., Hampson, G.J., Helland-Hansen, W., Johannessen, E.P., Steel, R.J., 2009. Shelf
579 edge and shoreline trajectories, a dynamic approach to stratigraphic analysis. *Basin Res.* 21,
580 445–453. <https://doi.org/10.1111/j.1365-2117.2009.00432.x>

581 Hickson, T.A., Sheets, B.A., Paola, C., Kelberer, M., 2005. Experimental Test of Tectonic
582 Controls on Three-Dimensional Alluvial Facies Architecture. *J. Sediment. Res.* 75, 710–
583 722. <https://doi.org/10.2110/jsr.2005.057>

584 Holbrook, J., 2001. Origin, genetic interrelationships, and stratigraphy over the continuum of
585 fluvial channel-form bounding surfaces: An illustration from middle Cretaceous strata,
586 Southeastern Colorado. *Sediment. Geol.* 144, 179–222. [https://doi.org/10.1016/S0037-](https://doi.org/10.1016/S0037-0738(01)00118-X)
587 [0738\(01\)00118-X](https://doi.org/10.1016/S0037-0738(01)00118-X)

588 Kim, W., Muto, T., 2007. Autogenic response of alluvial-bedrock transition to base-level
589 variation: Experiment and theory. *J. Geophys. Res. Earth Surf.* 112, 1–13.
590 <https://doi.org/10.1029/2006JF000561>

591 Lai, S.Y.J., Capart, H., 2007. Two-diffusion description of hyperpycnal deltas. *J. Geophys. Res.*
592 *Earth Surf.* 112. <https://doi.org/10.1029/2006JF000617>

593 Lai, S.Y.J., Hsiao, Y.T., Wu, F.C., 2017. Asymmetric Effects of Subaerial and Subaqueous
594 Basement Slopes on Self-Similar Morphology of Prograding Deltas. *J. Geophys. Res. Earth*
595 *Surf.* 122, 2506–2526. <https://doi.org/10.1002/2017JF004244>

596 Li, Q., Yu, L., Straub, K.M., 2016. Storage thresholds for relative sea-level signals in the
597 stratigraphic record. *Geology* 44, 179–182.

598 Lorenzo-Trueba, J., Voller, V.R., 2010. Analytical and numerical solution of a generalized
599 Stefan problem exhibiting two moving boundaries with application to ocean delta
600 formation. *J. Math. Anal. Appl.* 366, 538–549. <https://doi.org/10.1016/j.jmaa.2010.01.008>

601 Lorenzo-Trueba, J., Voller, V.R., Muto, T., Kim, W., Paola, C., Swenson, J.B., 2009. A
602 similarity solution for a dual moving boundary problem associated with a coastal-plain
603 depositional system. *J. Fluid Mech.* 628, 427–443.
604 <https://doi.org/10.1017/S0022112009006715>

605 Lorenzo-Trueba, J., Voller, V.R., Paola, C., 2013. A geometric model for the dynamics of a
606 fluvially dominated deltaic system under base-level change. *Comput. Geosci.* 53, 39–47.
607 <https://doi.org/10.1016/j.cageo.2012.02.010>

608 Lorenzo-Trueba, J., Voller, V.R., Paola, C., Twilley, R.R., Bevington, A.E., 2012. Exploring the
609 role of organic matter accumulation on delta evolution. *J. Geophys. Res. Surf.* 117, F00A02.
610 <https://doi.org/10.1029/2012JF002339>

611 Marr, J.G., Swenson, J.B., Paola, C., Voller, V.R., 2000. A two-diffusion model of fluvial
612 stratigraphy in closed depositional basins. *Basin Res.* 12, 381–398.
613 <https://doi.org/10.1111/j.1365-2117.2000.00134.x>

614 Martin, J., Cantelli, A., Paola, C., Blum, M., Wolinsky, M., 2011. Quantitative Modeling of the
615 Evolution and Geometry of Incised Valleys. *J. Sediment. Res.* 81, 64–79.
616 <https://doi.org/10.2110/jsr.2011.5>

617 Martin, J., Paola, C., Abreu, V., Neal, J., Sheets, B., 2009. Sequence stratigraphy of experimental
618 strata under known conditions of differential subsidence and variable base level. *Am.*
619 *Assoc. Pet. Geol. Bull.* 93, 503–533. <https://doi.org/10.1306/12110808057>

620 Muto, T., 2001. Shoreline autoretreat substantiated in flume experiments. *J. Sediment. Res.* 71,
621 246–254. <https://doi.org/10.1306/091400710246>

622 Muto, T., Steel, R.J., 2002. Role of autoretreat and A/S changes in the understanding of deltaic
623 shoreline trajectory: A semi-quantitative approach. *Basin Res.* 14, 303–318.
624 <https://doi.org/10.1046/j.1365-2117.2002.00179.x>

625 Paola, C., 2000. Quantitative models of sedimentary basin filling. *Sedimentology.*
626 <https://doi.org/10.1046/j.1365-3091.2000.00006.x>

627 Paola, C., Heller, P.L., Angevine, C.L., 1992. The large-scale dynamics of grain-size variation in
628 alluvial basins, 1: Theory. *Basin Res.* 4, 73–90. [https://doi.org/10.1111/j.1365-](https://doi.org/10.1111/j.1365-2117.1992.tb00145.x)
629 [2117.1992.tb00145.x](https://doi.org/10.1111/j.1365-2117.1992.tb00145.x)

630 Paola, C., Voller, V.R., 2005. A generalized Exner equation for sediment mass balance. *J.*
631 *Geophys. Res. Earth Surf.* 110, 1–8. <https://doi.org/10.1029/2004JF000274>

632 Parker, G., Muto, T., 2003. 1D numerical model of delta response to rising sea level. 3rd IAHR
633 *Symp. River, Coast. Estuar. Morphodynamics* 1–10.

634 Parker, G., Muto, T., Akamatsu, Y., Dietrich, W.E., Lauer, J.W., 2008. Unravelling the
635 conundrum of river response to rising sea-level from laboratory to field. Part I: Laboratory
636 experiments. *Sedimentology* 55, 1643–1655. [https://doi.org/10.1111/j.1365-](https://doi.org/10.1111/j.1365-3091.2008.00961.x)
637 [3091.2008.00961.x](https://doi.org/10.1111/j.1365-3091.2008.00961.x)

638 Posamentier, H.W., Allen, H.W., James, D.P., Tesson, M., 1992. Forced regression in a sequence
639 stratigraphic framework: Concepts, examples, and sequence stratigraphic significance. *Am.*
640 *Assoc. Pet. Geol. Bull.* 76, 1687–1709.

641 Posamentier, H.W., Vail, P.R., 1988. Eustatic Controls on Clastic Deposition IH—Sequence and
642 Systems Tract Models. *Sea-Level Chang.* 42, 125–154.
643 <https://doi.org/10.2110/pec.88.01.0125>

644 Postma, G., Kleinhans, M.G., Meijer, P.T.H., Eggenhuisen, J.T., 2008. Sediment transport in
645 analogue flume models compared with real-world sedimentary systems: A new look at
646 scaling evolution of sedimentary systems in a flume. *Sedimentology* 55, 1541–1557.
647 <https://doi.org/10.1111/j.1365-3091.2008.00956.x>

648 Strong, N., Paola, C., 2008. Valleys That Never Were: Time Surfaces Versus Stratigraphic
649 Surfaces. *J. Sediment. Res.* 78, 579–593.

650 Swenson, J.B., Muto, T., 2007. Response of coastal plain rivers to falling relative sea-level:
651 Allogenic controls on the aggradational phase. *Sedimentology* 54, 207–221.
652 <https://doi.org/10.1111/j.1365-3091.2006.00830.x>

653 Swenson, J.B., Paola, C., Pratson, L., Voller, V.R., Murray, A.B., 2005. Fluvial and marine
654 controls on combined subaerial and subaqueous delta progradation: Morphodynamic
655 modeling of compound-cliniform development. *J. Geophys. Res. Earth Surf.* 110, 1–16.
656 <https://doi.org/10.1029/2004JF000265>

657 Swenson, J.B., Voller, V.R., Paola, C., Parker, G., Marr, J.G., 2000. Fluvio-deltaic
658 sedimentation: A generalized Stefan problem. *Eur. J. Appl. Math.* 11, 433–452.

659 <https://doi.org/10.1017/S0956792500004198>

660 Törnqvist, T.E., Wortman, S.R., Mateo, Z.R.P., Milne, G.A., Swenson, J.B., 2006. Did the last
661 sea level lowstand always lead to cross-shelf valley formation and source-to-sink sediment
662 flux? *J. Geophys. Res. Earth Surf.* 111. <https://doi.org/10.1029/2005JF000425>

663 van Heijst, M.W.I.M., Postmal, G., 2001. Fluvial response to sea-level changes: A quantitative
664 analogue, experimental approach. *Basin Res.* 13, 269–292. [https://doi.org/10.1046/j.1365-](https://doi.org/10.1046/j.1365-2117.2001.00149.x)
665 [2117.2001.00149.x](https://doi.org/10.1046/j.1365-2117.2001.00149.x)

666 Van Wagoner, J.C., Bertram, G.T., 1995. *Sequence Stratigraphy of Foreland Basin Deposits.*
667 *Memoir 64*, 487.

668 Van Wagoner, J.C., Mitchum, R.M.J., Campion, K.M., Rahmanian, V.D., 1990. Siliciclastic
669 *Sequence Stratigraphy in Well Logs, Cores and Outcrops.* AAPG Methods Explor. Ser. 7,
670 1–55.

671 Voller, V.R., Swenson, J.B., Kim, W., Paola, C., 2006. An enthalpy method for moving
672 boundary problems on the earth's surface. *Int. J. Numer. Methods Heat Fluid Flow* 16, 641–
673 654. <https://doi.org/10.1108/09615530610669157>

674 Voller, V.R., Swenson, J.B., Paola, C., 2004. An analytical solution for a Stefan problem with
675 variable latent heat. *Int. J. Heat Mass Transf.* 47, 5387–5390.
676 <https://doi.org/10.1016/j.ijheatmasstransfer.2004.07.007>

677

678

679

680

681

682

683

684

685

686 **Tables**

687 Table 1. State Variables and their Dimensions

Symbol	Units	Description	Dimensionless symbol
t	T	Time	t
x	L	Horizontal distance	x
h	L	Height above current sea-level	h
r	L	Alluvial-bedrock transition horizontal distance from origin	r
s	L	Shoreline horizontal distance from origin	s
q	$L^2 \cdot T^{-1}$	Sediment flux	q
Z	L	Sea-level	Z
H	-	Enthalpy	H
E	L	Basement elevation	E

688

689 Table 2. Description of the input parameters and their dimensionless groups

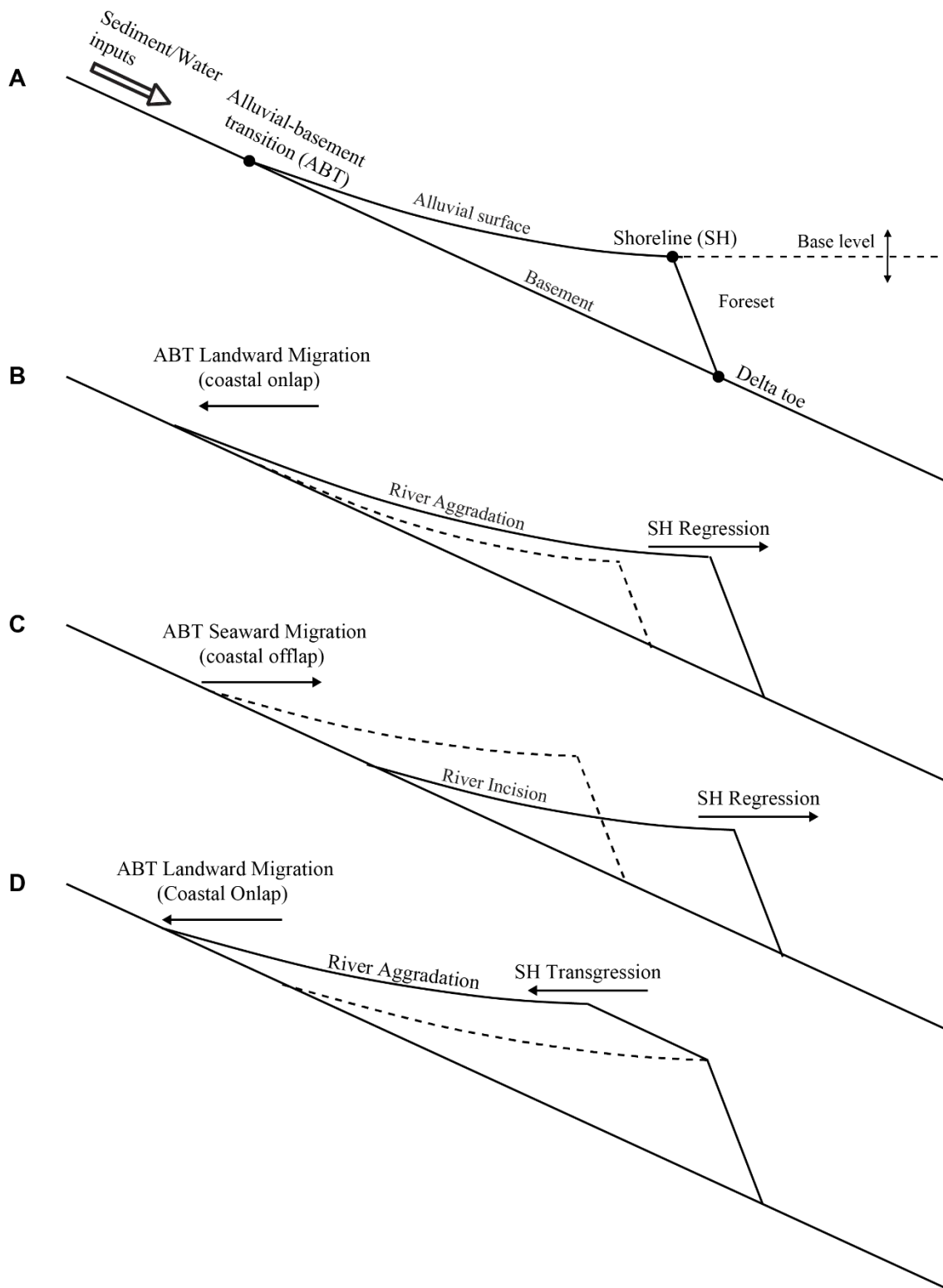
Symbol	Units	Description	Dimensionless symbol
q_0	$L^2 \cdot T^{-1}$	Sediment flux at ABT	R_{ab}
v	$L^2 \cdot T^{-1}$	Fluvial diffusivity	
β	-	Basement slope	

Ψ	-	Foreset slope	R_{sh}
\dot{z}	L·T ⁻¹	Rate of sea-level rise	\dot{z}
A	L	Amplitude of sea-level oscillations	A
B	T ⁻¹	Frequency of sea-level oscillations	B

690

691

692 **Figures**



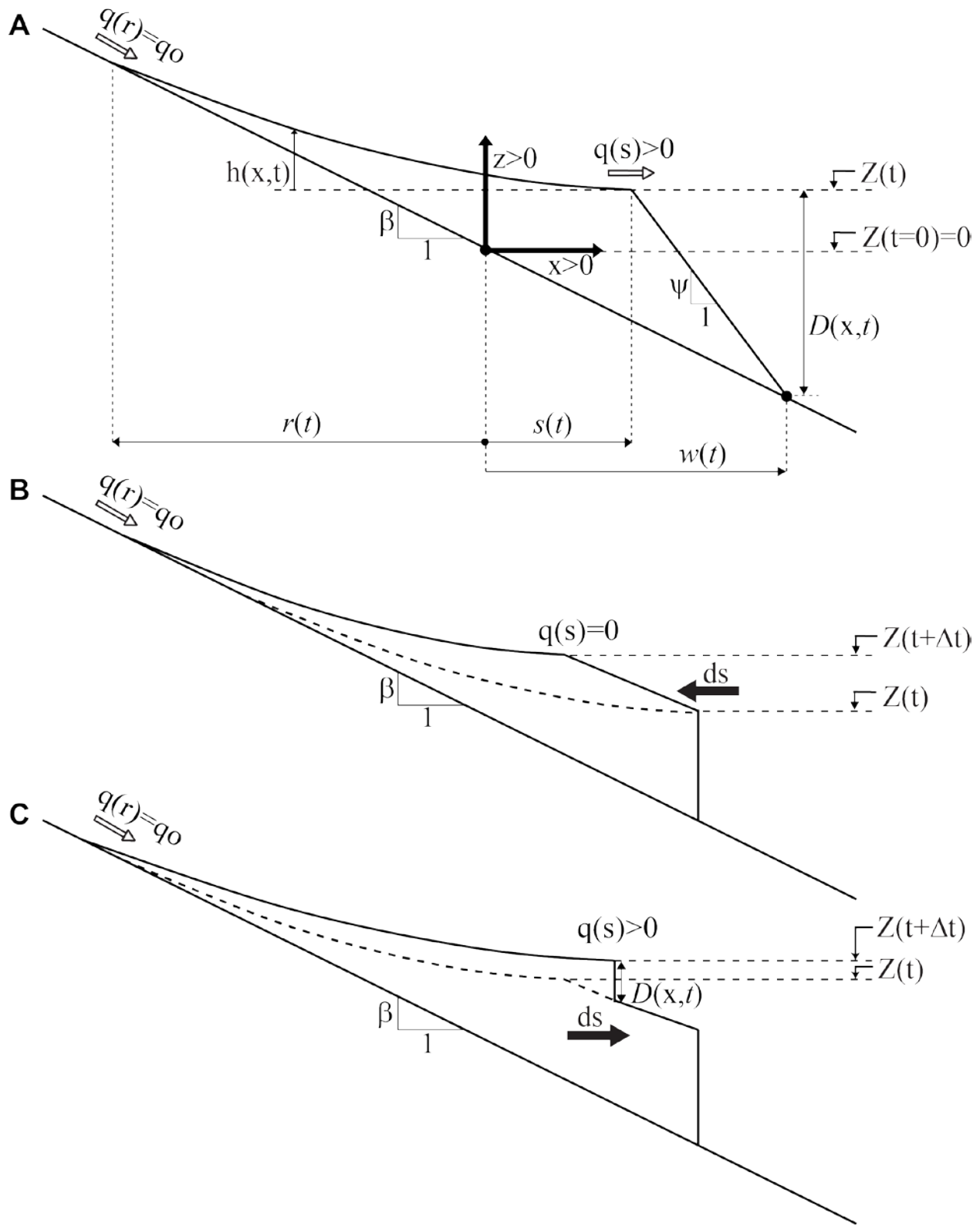
693

694 **Figure 1.** Conceptual sketches of the fluvio-deltaic system illustrating (a) geomorphic moving
 695 boundaries and key components, and (b)-(d) shoreline regression/transgression, coastal
 696 onlap/offlap at the ABT, and river aggradation/incision. Note the strong exaggeration of the
 697 vertical scale.

698

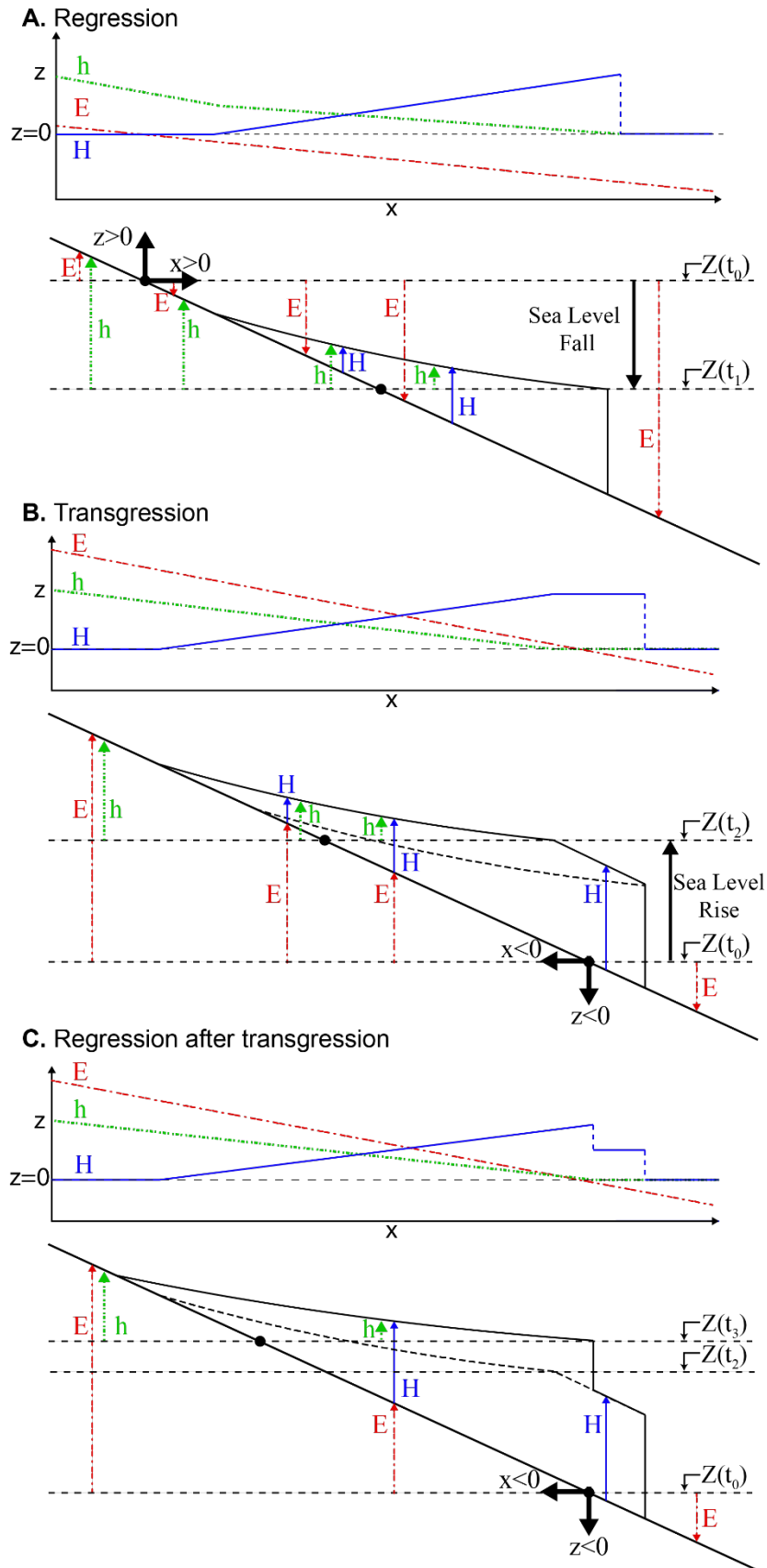
699

700



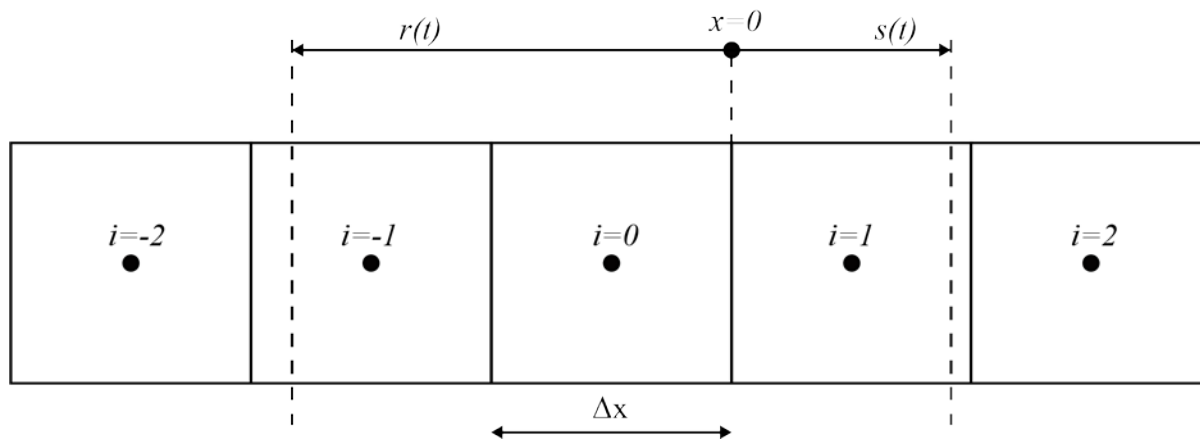
701

702 **Figure 2.** (a) Model setup, including state variables. (b) Sketch for autobreak. (c) Sketch for
 703 shoreline regression after autobreak



706 **Figure 3.** Model variables, including the enthalpy function H , the basement elevation E , and the
 707 fluvial surface elevation respect to the current sea level h , under (a) sea-level fall and SH
 708 regression, (b) sea-level rise and SH transgression, and (c) SH regression after autobreak.

709



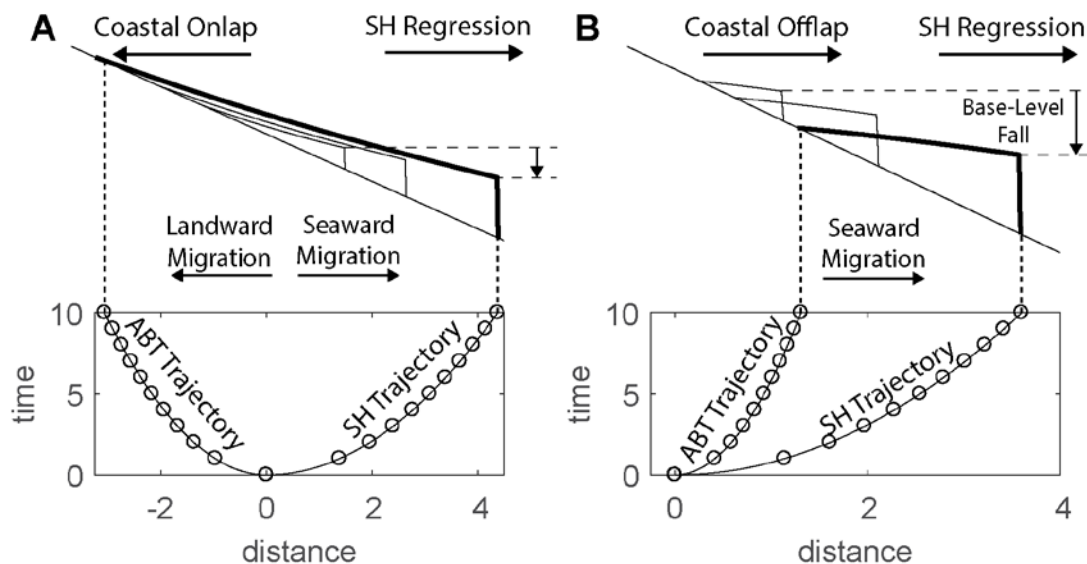
710

711

712 **Figure 4.** Sketch of discrete domain. In general the locations of the SH and the ABT, s and r
 713 respectively, are in between two nodes of our discrete domain.

714

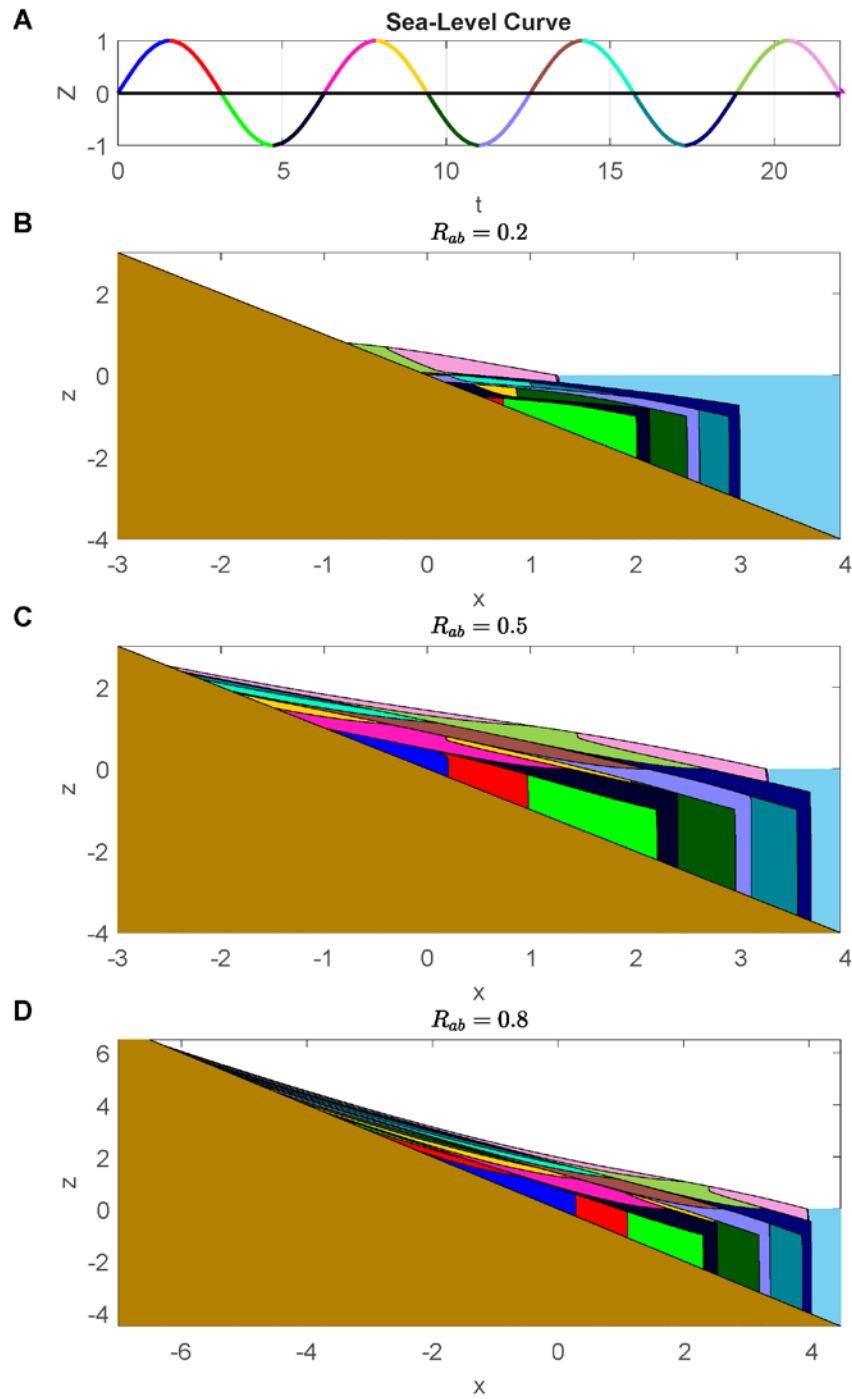
715



716

717 **Figure 5.** Model runs under square root sea-level fall with (a) $R_{ab} = 0.8$, $\lambda_z = -0.3$, and (b)
 718 $R_{ab} = 0.2$, $\lambda_z = -0.3$. At the bottom, we include a comparison of boundary trajectories of the
 719 analytical (solid-lines) and numerical (circles) solutions. At the top, we depict the evolution of
 720 the longitudinal profile over time.

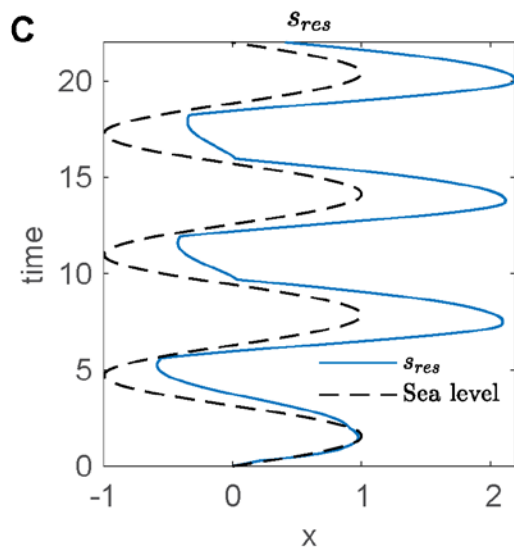
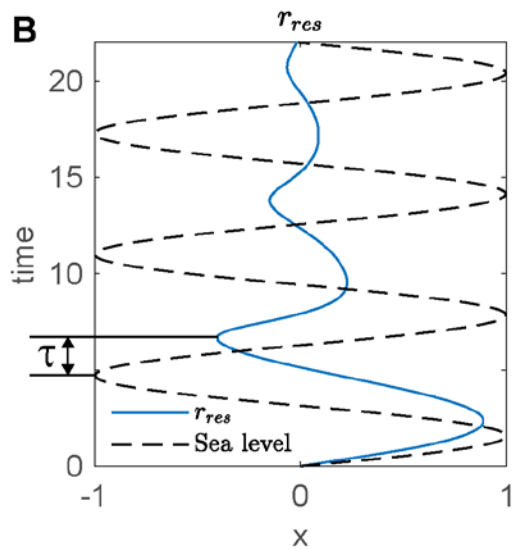
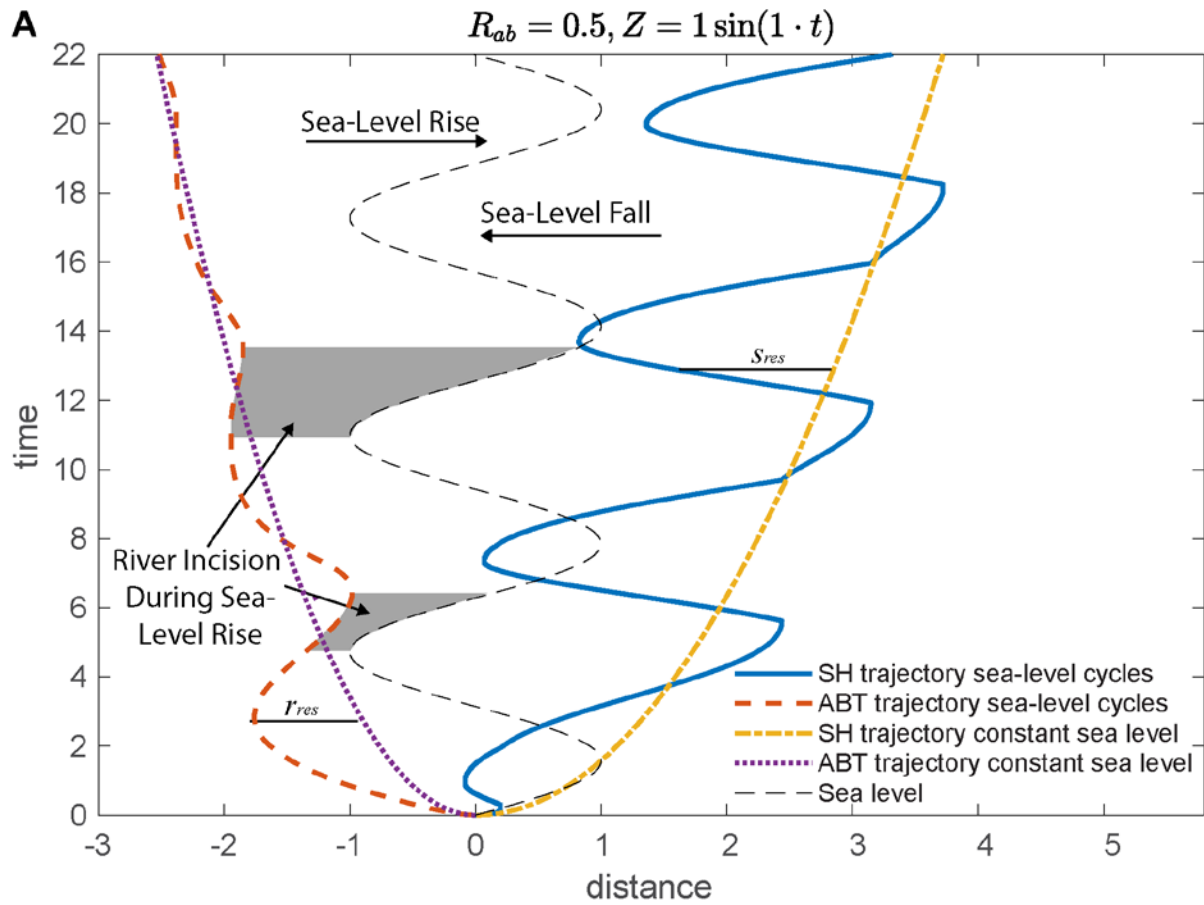
721



723

724 **Figure 6.** Stratigraphies produced under sea-level cycling for three different values of the
 725 dimensionless group $R_{ab} = q_0/(\beta v)$. Videos showing the evolution over time are available in
 726 the supplementary material.

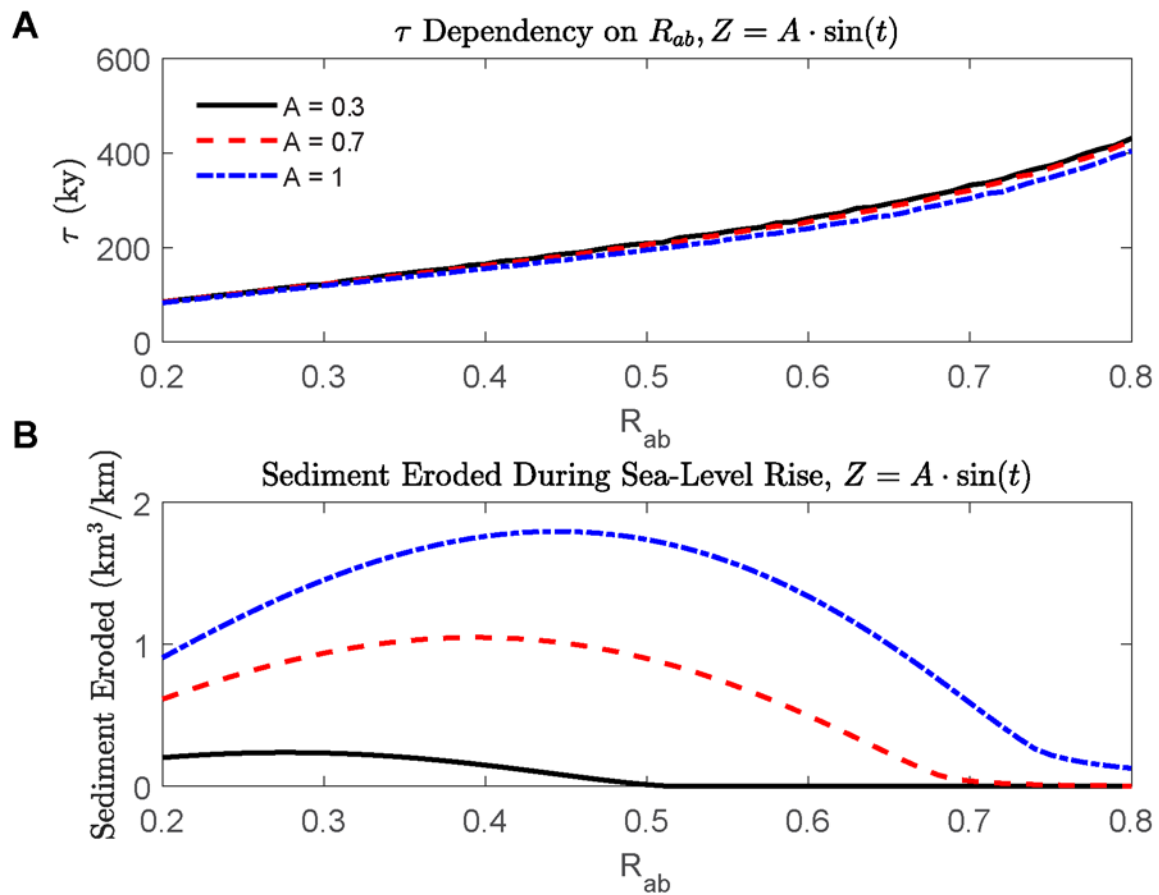
727



728

729 **Figure 7.** (a) ABT and SH trajectories under sea-level cycles (i.e., $Z = \sin(t)$) and $R_{ab} = 0.5$.
 730 Shaded intervals correspond to intervals of river incision during sea-level rise. (b) Plot of ABT
 731 residuals, r_{res} , and defining the time lag τ , as a function of the ABT residual. (c) Plot of SH
 732 residuals, s_{res} .

733



734

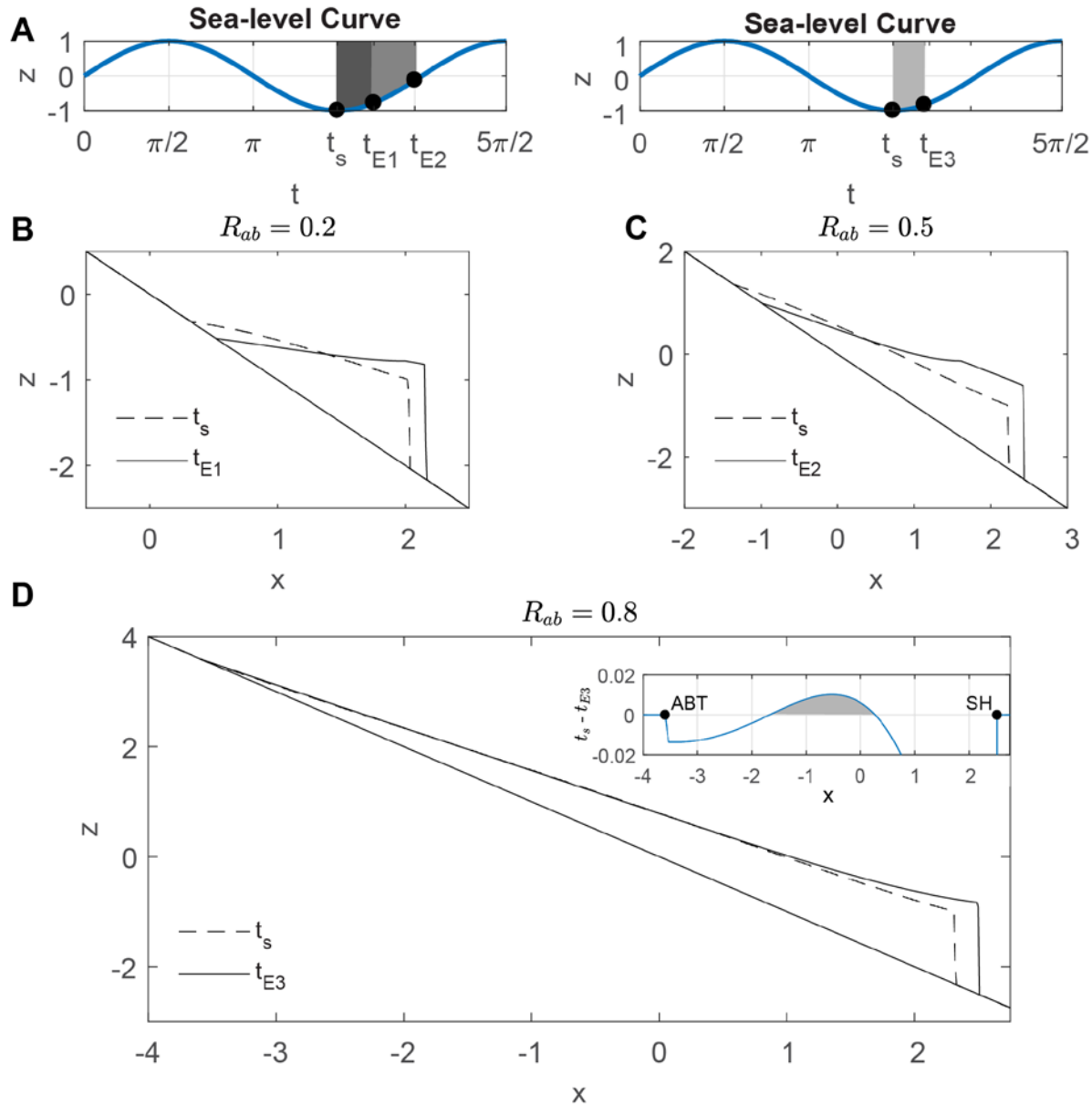
735 **Figure 8.** (a) Values for the delay in ABT response to sea-level rise as a function of the
 736 dimensionless group $R_{ab} = q_0/(\beta v)$, and the amplitude of the sea-level cycles A . (b) Sediment
 737 volume eroded during sea-level rise, also as a function of R_{ab} and A .

738

739

740

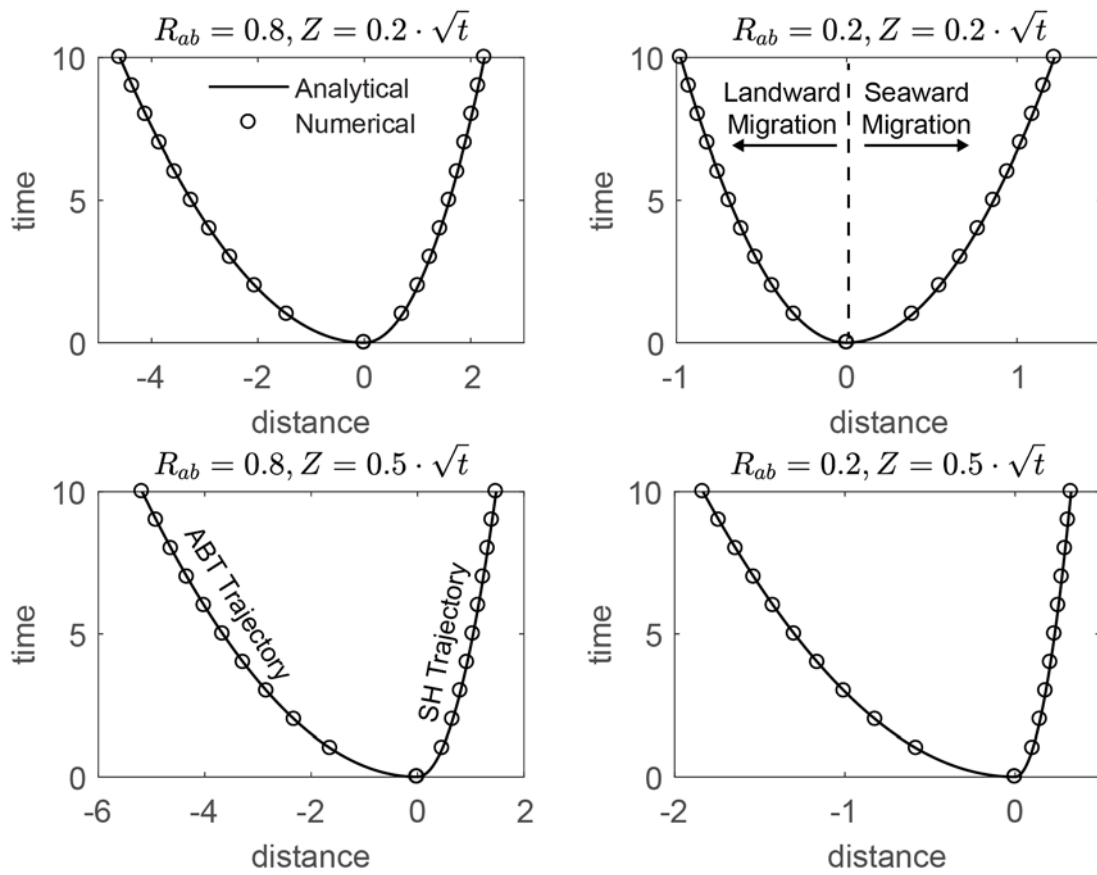
741



742

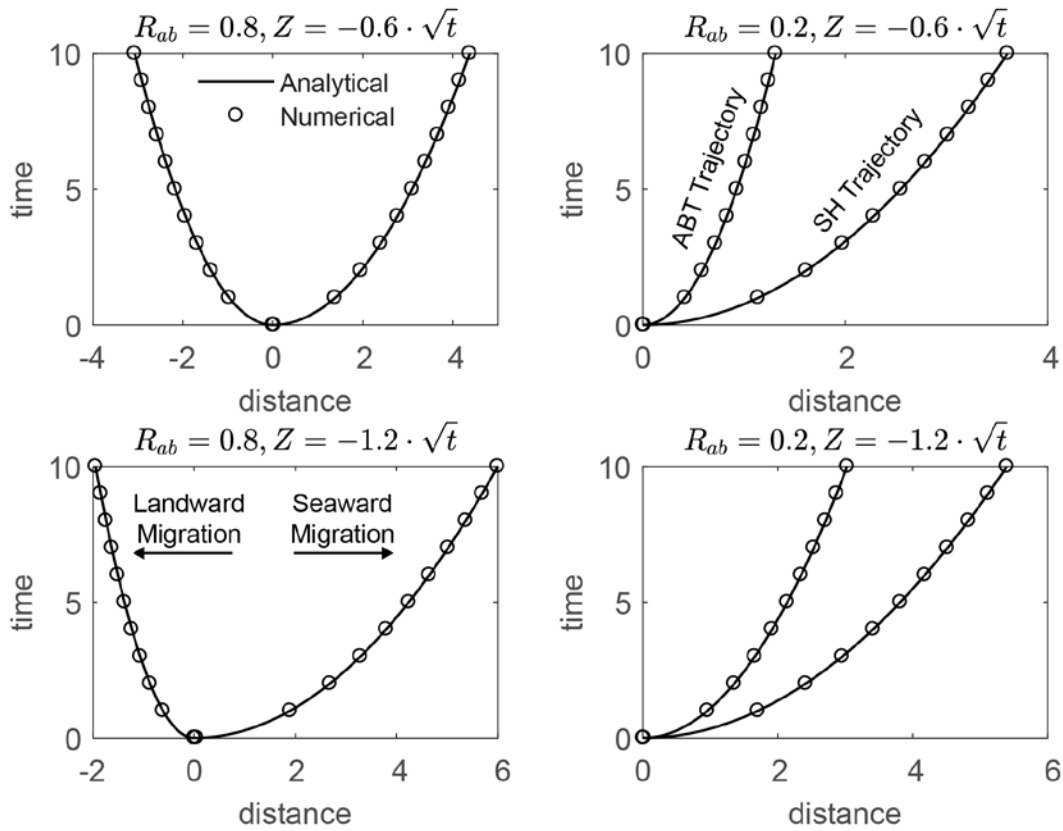
743 **Figure 9.** a) Sea-level curves showing the times for the onset of sea-level rise t_s , and at the
 744 conclusion of river incision under sea-level rise for different R_{ab} values (i.e., t_{E1} for $R_{ab} = 0.2$,
 745 t_{E2} for $R_{ab} = 0.5$, and t_{E3} for $R_{ab} = 0.8$). Below, longitudinal profiles depicting the sections at
 746 the onset of sea-level rise (dashed line), and at the conclusion of river incision under sea-level
 747 rise (solid line) under (b) $R_{ab} = 0.2$, (c) $R_{ab} = 0.5$, and (d) $R_{ab} = 0.8$. Note that under $R_{ab} =$
 748 0.8 , although the ABT does not migrate seawards, sediment erodes from the mid portion of the
 749 fluvial surface during sea-level rise. The stratigraphic profiles for the three model runs are
 750 included in Figure 6, and the ABT and SH trajectories for the $R_{ab} = 0.5$ scenario are included in
 751 Figure 7a.

752



754

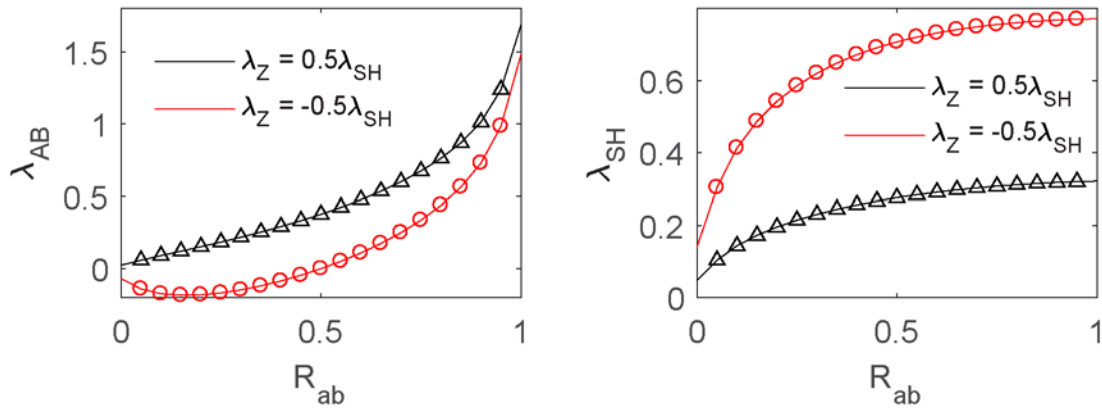
755 **Figure A1.** Comparison of analytical (solid lines) and numerical (circles) ABT and SH
 756 trajectories under square-root sea-level rise.



757

758 **Figure A2.** Comparison of analytical (solid lines) and numerical (circles) ABT and SH
 759 trajectories under square-root sea-level fall.

760

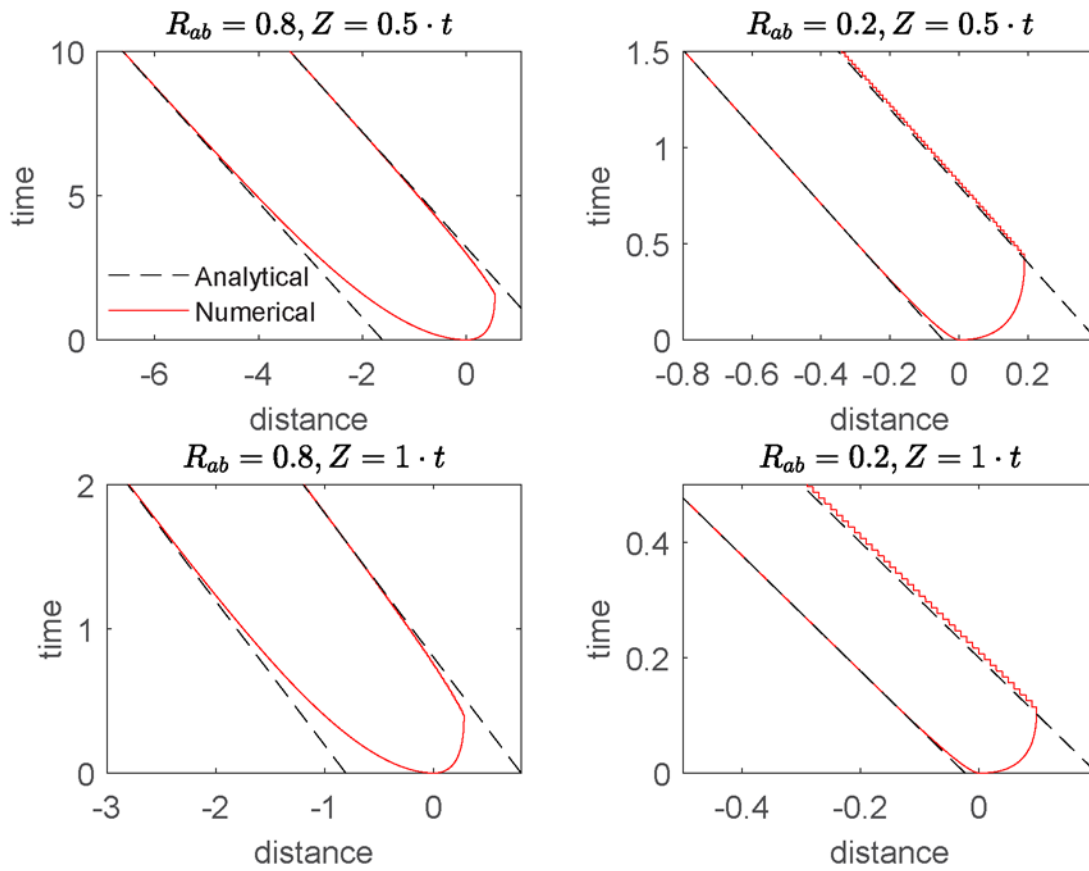


761

762 **Figure A3.** Comparison between analytical and numerical predictions of the moving boundary
 763 parameters λ_{sh} and λ_{ab} for the sea-level fall (circles) and sea-level rise (triangles) scenarios. The
 764 solid-line is the analytical solution and the symbols represent the enthalpy numerical solution
 765 described in section 4. We use $\Delta x = 0.01$ and $\Delta t = 5 \cdot 10^{-5}$.

766

767

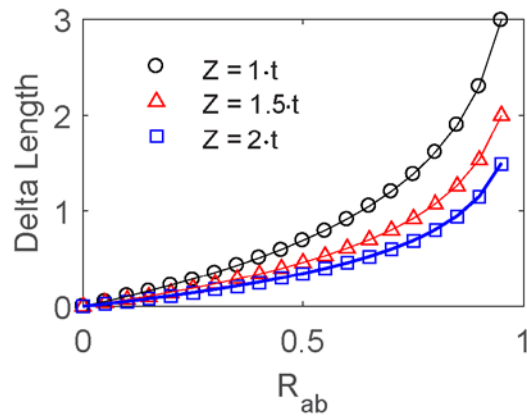


768

769 **Figure A4.** Comparison of analytical (dashed) and numerical (solid) ABT and SH trajectories
770 under constant sea-level rise with $\Delta x = 0.01$ and $\Delta t = 5 \cdot 10^{-5}$.

771

772



773

774 **Figure A5.** Comparison of analytical (solid lines) and numerical (symbols) delta length values
775 (i.e., $s - r$) at steady state.

776

777

778